The onset of fabric development in deep marine sediments

Maffione, Marco; Morris, Antony

DOI:
10.1016/j.epsl.2017.06.018

Highlights

- High-resolution AMS study of deep marine clay-rich sediments from IODP Site U1438
- Compaction-related fabrics initiate sharply at 83 mbsf (5.7 Ma after deposition)
- Fabrics continue to form over a 6 Ma long, 30 m thick ‘initial compaction window’
- An effective stress threshold triggers compaction-related fabric development

The onset of fabric development in deep marine sediments

Marco Maffione[1,2] and Antony Morris[3]

[1]School of Geography, Earth and Environmental Sciences, University of Birmingham, Edgbaston, Birmingham, B15 2TT, UK

[2]Department of Earth Sciences, Utrecht University, Heidelberglaan 2, 3584 CS Utrecht, Netherlands

[3]School of Geography, Earth and Environmental Sciences, Plymouth University, Drake Circus, Plymouth, PL4 8AA, UK

Keywords

Sedimentary fabric; deep marine; compaction; magnetic anisotropy; AMS; International Ocean Discovery Program

Abstract

Post-depositional compaction is a key stage in the formation of sedimentary rocks that results in porosity reduction, grain realignment and the production of sedimentary fabrics. The progressive time-depth evolution of the onset of fabric development in deep marine sediments is poorly constrained due to the limited quantity and resolution of existing data. Here we present high-resolution anisotropy of magnetic susceptibility (AMS) results from clay-rich deep marine sediments recovered at International Ocean Discovery Program Site U1438 (Philippine Sea). AMS is a petrofabric tool sensitive to the preferred orientation of grains in rocks. Down-section variations of AMS parameters, density, porosity and the inclination of magnetic remanences demonstrate that fabrics develop in response to compaction and dewatering but also that they do not develop progressively with depth below the mudline. Instead, a horizontal foliation first forms at 83 mbsf once the sediment load reaches an effective stress threshold for the onset of compaction and is then continuously enhanced down to 113 mbsf, defining a 30 m-thick 'initial compaction window'. The magnetostratigraphic age model for IODP Site U1438 indicates a delay of 5.7 Ma in initial fabric formation following sediment deposition, with strongly defined fabrics then taking an additional 6.5 Ma to develop.

1. Introduction

During deposition of (hemi)pelagic sediments in deep-sea environments, platy minerals (mainly phyllosilicates) tend to align with their long axes parallel to the water-sediment interface. Bottom-current disturbance and bioturbation, together with the natural predisposition of clay flakes to form edge-to-edge and edge-to-face contacts due to surface electric charge distribution (Bennett et al., 1991), eventually result in an uppermost sedimentary interval characterized by a chaotic internal structure (i.e., isotropic fabric) and high porosity and water content (Bennett et al., 1991; Reynolds and Gorsline, 1992). With increasing vertical burial load at depth, clays particles rotate to form horizontal face-to-face contacts, accompanied by simultaneous dewatering and porosity reduction (Bennett et al., 1981; Bennett and Hulbert, 1986). The effect of this process on the microstructure of the sediment is the formation of a fabric characterized by a well-defined horizontal foliation plane.

The majority of dewatering and compaction in pelagic sedimentary sequences is thought to occur progressively within the uppermost stratigraphic intervals (e.g., Arason and Levi, 1990). However, only a few previous studies have investigated microstructure changes during compaction and initial fabric development in deep marine environments (Kopf and Behrmann, 1997; Hirano et al., 2001; Kawamura and Ogawa, 2002; 2004), and none have a sufficiently high spatial and temporal resolution to describe in detail the evolution of this process. Here we present results of a high-resolution anisotropy of magnetic susceptibility (AMS) analysis of a sequence of unconsolidated deep marine sediments recovered in the Philippine Sea by International Ocean Discovery Program (IODP) Expedition 351 (Arculus et al., 2015a), where magnetostratigraphy provides an accurate age model. We use AMS as a sensitive measure of fabric development in these sediments (e.g., Rochette et al., 1992; Tarling and Hrouda, 1993; Borradaile and Jackson, 2004), and compare magnetic fabric parameters with other physical properties to tightly constrain the depth and timing of the onset and evolution of fabric development in a deep marine environment.

2. Geological background and sampling

2.1. Tectonic framework of the Philippine Sea Plate and IODP Site U1438

The Philippine Sea Plate (PSP) is an oceanic plate located between the Eurasia and Pacific plates and bordered by active subduction zones (Figure 1). The PSP can be subdivided into three tectono-stratigraphic domains: (i) a western domain floored by a complex array of oceanic plateaux, ridges, and basins of Cretaceous to Oligocene age and bordered to the east by the Eo-Oligocene (~55-

25 Ma) Kyushu-Palau Ridge (e.g., Deschamps and Lallemand, 2003; Okino and Fuijoka, 2003; Ishizuka et al., 2011a, 2013); (ii) a central domain dominated by the Miocene (~25-12 Ma) Parece Vela-Shikoku back-arc basin (Okino et al., 1994) occurring between the Kyushu-Palau Ridge and the modern Izu-Bonin-Mariana (IBM) arc; and (iii) an eastern domain forming the forearc region between the modern IBM arc and the IBM trench, developed upon initiation of subduction of the Pacific plate below the PSP at ~52 Ma (Ishizuka et al., 2011b; Reagan et al., 2010; Arculus et al., 2015b).

During June and July 2014, IODP Expedition 351 (Arculus et al., 2015a) recovered a suite of sedimentary and volcanic rocks at Site U1438 (4700 m water depth) in the western domain of the PSP (Amami Sankaku Basin; 27.38°N, 134.32°E; Figure 1a). Four progressively deeper holes were drilled at this site, down to 26.5, 257.3, 897.8, and 1611 metres below seafloor (mbsf), at Holes U1438A, B, D and E respectively. Recovered rocks (Figure 1b) consist of a thick sedimentary sequence (Units I-IV) deposited since the Early Eocene (~55 Ma) and recording the birth, evolution and death of the Kyushu-Palau Ridge, overlying igneous basement rocks (Unit 1).

2.2. Deep marine sedimentation in the west PSP (Unit I)

Unit I (0-160.3 mbsf; Hole U1438B) is an unconsolidated fine-grained pelagic and hemipelagic sedimentary sequence composed of mud, tuffaceous mud, mud with ash, and clay with discrete ash beds. Paleomagnetic and biostratigraphic constraints place the base of Unit I at the Miocene-Oligocene transition (Arculus et al., 2015a). Deposition of Unit I therefore started soon after the demise of Kyushu-Palau Ridge volcanism and initial opening of the Parece Vela-Shikoku back-arc basin to the east (thought to occur at ~25 Ma; Okino et al., 1994). Since no significant tectonic events occurred since that time at the location of Site U1438, Unit I represents the product of deep marine sedimentation, with sedimentation rates ranging from ~2 to ~0.5 cm/kyr (Arculus et al., 2015a). The average grain size of Unit I changes slightly down-core, with the uppermost interval (0-45 mbsf) mainly represented by siltstones with a significant (up to 60%) biogenic, mainly siliceous component, a central interval (45-93 mbsf) dominated by claystones with a lower biogenic content, and a bottom interval (93-160.3 mbsf) represented again predominantly by siltstones. Bioturbation is rare in the upper interval of Unit I (< 93 mbsf) and increases at depth, with more bioturbated intervals occurring below 121 mbsf. X-Ray diffraction analyses revealed a predominant assemblage of quartz, plagioclase, chlorite, muscovite, illite and other clay minerals (Arculus et al., 2015a). Below ~93 mbsf (in the lower siltstones) quartz content decreases, while the content of zeolite and clay minerals increases.

3. Methods

Anisotropy of magnetic susceptibility (AMS) is a petrofabric tool used to determine the preferred orientation of minerals (e.g., Jelínek, 1981; Hrouda, 1982; Borradaile, 1988; Rochette et al., 1992; Tarling and Hrouda, 1993; Borradaile and Jackson, 2004). AMS is geometrically described by an ellipsoid with principal axes corresponding to the minimum (k_{min}), intermediate (k_{int}), and maximum (k_{max}) susceptibilities (Hrouda, 1982). The relative magnitude of the susceptibility axes defines the shape of the AMS ellipsoid, which can be: (1) isotropic ($k_{\mathrm{min}} = k_{\mathrm{int}} = k_{\mathrm{max}}$) when grains are not aligned preferentially; (2) oblate

($k_{\min} << k_{\text{int}} \approx k_{\max}$) when grain alignment defines a foliation plane; (3) triaxial ($k_{\min} < k_{\text{int}} < k_{\max}$) when grain alignment results in a well-defined foliation and a lineation; or (4) prolate ($k_{\min} \approx k_{\text{int}} << k_{\max}$) when grain alignment defines a lineation. Here we describe the strength of anisotropy using the corrected anisotropy degree (P_J; Jelínek,1978), where P_J = 1.0 indicates an isotropic fabric and, e.g., P_J = 1.05 indicates 5% anisotropy. The shape of the ellipsoid is described by the shape parameter (T), where -1.0 < T < 1.0 and positive/negative values of T indicate oblate/prolate fabrics respectively (Jelínek 1978).

Sedimentary fabrics are characterised by P_J > 1.0, oblate AMS ellipsoids (0 < T < 1), vertical k_{min} axes, and k_{int} and k_{max} axes dispersed within the horizontal foliation plane.

We measured the anisotropy of low-field magnetic susceptibility of 173 discrete, 8 cm^3 cubic samples from the top 140 m of Unit I. Measurements were carried out using an AGICO KLY-3S Kappabridge (Plymouth University), and susceptibility tensors and associated eigenvectors and eigenvalues calculated using AGICO Anisoft 4.2 software. Instrument precision for AMS measurements for the KLY-3S system is > 99%, yielding meaningful principal directions in weakly anisotropic rocks when P_J > 1.003 (Burmeister et al., 2009). Sample orientations were determined by correcting cores recovered from Hole U1438B to the geographic reference frame using "FlexIT" tool data obtained during advanced piston corer (APC) deployments (Arculus et al., 2015a).

Rock magnetic experiments were performed to investigate the nature of the mineral fractions contributing to the AMS. Curie temperatures were determined from the high-temperature (20-700°C) variation of magnetic susceptibility of representative samples, measured using a KLY-3S coupled with a CS-3 high-temperature furnace apparatus. Isothermal remanent magnetization (IRM) acquisition experiments were conducted on representative samples using a Molspin pulse magnetizer to apply peak fields up to 800 mT with resulting IRMs measured using an AGICO JR6A spinner magnetometer.

Finally, we also employ shipboard paleomagnetic and physical property data from Hole U1438B, collected using methods documented in Arculus et al. (2015a).

4. Results

AMS parameters from the investigated interval of Unit I are extremely variable with depth, with a clear change occurring at 83 mbsf (Figure 2; Supplementary material Table 1). The anisotropy degree is low (P_J ≈1.006) indicating weakly anisotropic sediments in the uppermost 83 m of the sequence, but progressively increases over an interval of ~30 m below 83 mbsf, reaching a maximum of P_J ≈1.060 at 113 mbsf (Figure 2a). Similarly the shape parameter (T) is extremely variable from -1.0 to +1.0 in the upper interval, becoming consistently oblate ($0.6 < T < 1.0$) immediately below 83 mbsf, and then strongly oblate ($0.8 < T < 1.0$) below 113 mbsf (Figure 2b). In addition, the orientation of the principal susceptibility axes changes with depth. Above 83 mbsf, magnetic fabrics are randomly oriented, with only the k_{min} axes showing a faint alignment near the vertical (Figure 3a). Below 83 mbsf, k_{min} axes become tightly clustered along the vertical, and the k_{int} and k_{max} axes align with the horizontal plane (Figure 3b). A weak clustering of k_{max} axes along an ESE-NWN orientation is also observed, potentially reflecting weak bottom water currents during deposition (Hrouda and Jezek, 1999). Mean magnetic susceptibility shows a slight increase with depth from ~30 to ~80 x 10^{-5} SI (Figure 2c).

Results from high-temperature variation of magnetic susceptibility experiments revealed consistent maximum Curie temperatures of ~580°C (Figure 4a), indicating that the ferromagnetic fraction in these sediments is dominated by near-stoichiometric magnetite (Dunlop and Özdemir, 1997). This is consistent with IRM acquisition experiments, where saturation was reached at applied fields of 200-300 mT (Figure 4b), consistent with the presence of low-coercivity, fine-grained (single-domain to pseudo-single-domain) magnetite. However, the vertical alignment of k_{min} axes (perpendicular to horizontal bedding in the sediments) indicates a dominance of normal sedimentary fabrics, and excludes the presence of significant inverse magnetic fabric components due to single domain effects in these sediments (Potter and Stephenson, 1988).

5. Discussion

5.1. Comparison of AMS fabric variations with physical properties

Interpretation of AMS data requires understanding of the source of the susceptibility signal and its potential variability downhole. A linear relationship between low field magnetic susceptibility and the intensity of natural remanent magnetization (NRM) suggests constancy of ferromagnetic mineralogy and grain-size (domain state) through Unit I (Figure 4c), implying that the contribution of magnetite to the susceptibility signal is controlled by concentration alone. The relatively low bulk magnetic susceptibility (Figure 2c), however, indicates that magnetite content is low and that the paramagnetic phyllosilicate matrix is likely the main contributor to susceptibility in these sediments, as typically observed in clay-rich sediments (e.g., Borradaile and Jackson, 2004; Sagnotti and Speranza, 1993; Maffione et al., 2012, 2015; Parés, 2015).

The rapid increase of the anisotropy degree, together with the acquisition of a consistently oblate fabric below 83 mbsf within Unit I (Figure 2) marks the onset of development of a horizontal foliation typical of sedimentary fabrics (Figure 3b). This foliation is progressively enhanced down to 113 mbsf, where the anisotropy degree reaches a maximum and AMS ellipsoids become strongly oblate (Figure 2b). This depth interval of fabric development coincides with a distinct decrease in porosity from 75 to 65% and increase in bulk density from ~1.45 to ~1.55 g/cm^3 (Figure 2d), seen in shipboard physical property data acquired on discrete samples analysed during IODP Expedition 351 (Arculus et al., 2015a). This suggests that fabrics have developed in response to mechanical compaction and dewatering occurring during burial diagenesis due to increasing effective overburden stress. Chemical compaction is considered insignificant in Unit I, as this generally only becomes a significant porosity-occluding process at depths greater than ~2 km (Bjørlykke and Høeg, 1997; Mondol et al., 2008). An apparent increase in sedimentation rate from ~0.5 to ~2.0 cm/ka at 83 mbsf (Figure 2e) is likely to also result from mechanical compaction rather than a change in rate of sediment supply.

5.2. Paleomagnetic evidence for compaction

As an additional test for the compaction-related origin of fabric development we analyzed the occurrence of inclination shallowing of paleomagnetic remanences, which characteristically results from compaction (e.g., Anson and Kodama, 1987;

Arason and Levi, 1990; Tauxe and Kent, 2004; Huang et al., 2013). Shipboard remanence directions are presented in Figure 5 (based on measurements of archive half core sections following alternating field demagnetization at 25 mT to remove significant drilling-induced components; Figure 6). Inclinations above 83 mbsf are close to the value expected at IODP Site U1438, but are generally shallower than expected below this (Figure 5a). To test this statistically, we selected only data from the bottom 1.0 m of each core in order to exclude intervals affected by drilling-induced shearing (commonly encountered in IODP piston cores (Acton et al., 2002) and evident in the declination data of Figure 5b). Mean inclinations were calculated after transposing all data to normal polarity and applying a fixed 45° cut-off to the distribution of corresponding virtual geomagnetic poles (following the methodology of Johnson et al. (2008)). For the uppermost 83 m of Unit I, the mean inclination of 44.1° (α_{95} = 1.2°, n = 408) is not statistically different from the expected geocentric axial dipole (GAD) inclination at this site (I = 46°). In contrast, the mean inclination below 83 mbsf (I = 39.7°; α_{95} = 1.8°, n = 266) is statistically significantly shallower. Using the elongation/inclination (E/I) correction method (Tauxe and Kent, 2004) we obtained an unflattened inclination for the interval 83-140 mbsf of 42.8° (95% confidence limits: 40.2°-53.4°) consistent with the expected inclination. These results further confirm that mechanical compaction has affected the lower interval of Unit I but is absent or not statistically significant at shallower depths.

5.3. Potential causes of the sudden onset of fabric development at 83 mbsf

5.3.1. Comparison with compaction trends for marine mudrocks

Effective stress-controlled mechanical compaction at the relative shallow depths of Unit I in Hole U1438B might be expected to produce continuous changes in physical properties, i.e. with a progressive decrease in porosity and increase in anisotropy degree with depth. Following Kopf and Behrmann (1997), we compare downhole porosity variations with published mechanical compaction functions by converting porosity determinations to uniaxial vertical shortening values, e_v using:

$$e_v = \frac{P_0 - P}{P - 100}$$

where P is a given sample porosity (in %) and P_0 is an initial porosity near the mudline (taken as 75%). Figure 7 compares the resulting values to converted porosity-depth trends for clays and claystones of Terzaghi (1925), Athy (1930), Hamilton (1976) and Sclater and Christie (1980). Though variable, each model predicts a smooth, monotonic increase in shortening with depth, in contrast to the stepwise increase at 83 mbsf in Unit I from e_v values close to zero (mean = -0.03) to a mean value of -0.21 below. This is consistent with the AMS data that show a uniformly low anisotropy degree down to 83 mbsf and then a sharp change in character to pronouncedly oblate fabrics. Hence, factors other than continuous compaction across the whole depth interval of Unit I must influence fabric development in these sediments.

5.3.2. Apparent overconsolidation

The sharp increase of the anisotropy degree in the studied unit resembles the pattern expected for "apparent overconsolidation" (Schwehr et al., 2006), whereby sediments appear more consolidated than predicted by simple burial for a given depth. According to Schwehr et al. (2006) apparent overconsolidation can result from unconformities produced by underwater landslides, which unload pre-consolidated sediments that then become buried by new sediments. Alternatively, overconsolidation can be caused by repeated shaking events (Locat and Lee, 2002). The continuous magnetostratigraphic record at Unit I (Arculus et al., 2015a), however, excludes the existence of unconformities within the sequence, and it is unlikely that seismic events only caused overconsolidation of the interval of Unit I below 83 mbsf without also affecting the top of the section in this tectonically active region.

5.3.3. Compositional control

Compaction of sediments can be controlled by variations in the composition and size of sedimentary grains, with, for example, platy hyllosilicate minerals tending to facilitate compaction. However, no major change in phyllosilicate mineralogy, grain size or degree of bioturbation of the mudrocks of Unit I (Arculus et al., 2015a) corresponds with the sharp onset of fabric development at 83 mbsf. Curtis et al. (1980) have demonstrated that although preferred orientations in clay-rich sediments commonly result from compactional strain, fabric development may be affected by the presence of non-platy silicate particles (such as quartz grains) which inhibit planar fabric development in their immediate vicinity. In this context, we note a downhole decrease in the volume percentage of fine-grained quartz particles in the mudrocks, from an average of 8% to 4% (based on smear-slide data collected during shipboard analyses; Arculus et al., 2015a). This minor compositional change is illustrated semi-quantitatively by variations in the intensity of quartz peaks at 26.6° 2 θ in XRD analyses of Unit I mud samples (Figure 2g; data from Arculus et al., 2015a). Quartz content, however, mainly decreases between 50 and 65 mbsf (Figure 2g), and remains constant throughout the interval where sharp variations of AMS parameters are observed. Furthermore, the volume percentage change in quartz affecting fabric development in the mudrocks analysed by Curtis et al. (1980) was much more dramatic (28% to 15%). Finally, the combined volume percentage of the main non-platy silicates (quartz plus feldspar) in Hole U1438B increases slightly from 12% to 15% across the interval where AMS fabrics develop (Arculus et al., 2015a), suggesting that this mechanism cannot account for the stepwise change in anisotropy observed here.

5.3.4. An effective stress threshold for the 'initial compaction window'

The stepwise variation of anisotropy parameters, porosity/vertical shortening and bulk density with depth documented here suggests that compaction and sedimentary fabric development is not progressive, but only starts once the burial load produces a sufficient effective stress to exceed the internal resistance to compaction represented by the friction along grain contacts during reorientation. In this case, the density data of Figure 2d, a water depth of 4700 m and a seawater density of 1029 kg/m^3 combine to yield an effective stress at 83 mbsf of 0.35 MPa (where effective stress = total stress – pore water pressure (assumed to be hydrostatic); Terzaghi, 1925). Sedimentary fabric in the studied section then develops over a restricted interval between 83 and 113 mbsf here defined as the 'initial compaction window', where pore reduction and preferred horizontal alignment of phyllosilicate flakes is progressively enhanced over a 30 m-thick interval. A similar compaction window can also be inferred in pelagic sediments from ODP Site 1149 in the NW Pacific Ocean, where a stepwise change in physical properties occurs between 118 and 150 mbsf (Kawamura and Ogawa, 2002; 2004).

5.4 Implications for fabric studies on deformed ancient mudrocks

The excellent age control at Site U1438, based on the IODP Expedition 351 shipboard magnetostratigraphy that successfully identified every geomagnetic chron in core sections back to 36 Ma (Arculus et al., 2015a), provides constraints on the timing of initial development of sedimentary fabrics in Unit I mudrocks. These indicate that the full process of fabric development documented here started 5.7 Ma after initial deposition and then took 6.5 Ma to complete (Figure 2e). This has implications for studies using AMS to document the progressive tectonic overprinting of sedimentary fabrics in ancient mudrocks (e.g., Sagnotti et al., 1998; Larrasoaña et al., 2004). Such studies typically assume that initial sedimentary fabrics (which are subsequently partially overprinted by tectonic fabrics) correspond to the biostratigraphic age of the sampled rocks. Instead results here suggest that a ~6 Ma hiatus between deposition and initial fabric development may need to be considered when documenting the evolution of anisotropy in deep marine mudrocks.

6. Conclusions

A detailed record of progressive fabric development in deep marine sediments sampled at IODP Site U1438 with robust age control indicates that a compaction-related horizontal foliation started to form 5.7 Ma after initial sedimentation (83 mbsf) and developed over the subsequent 6.5 Ma (down to 113 mbsf), within a

30 m-thick interval here termed the 'initial compaction window'. These new results provide the first high-resolution time/depth constraints on the onset of fabric development in deep marine environments, with implications for the tectonic application of AMS in pelagic sedimentary rocks. More data are now required from such deep marine environments to determine the variability in the onset of the initial compaction window, including additional quantification of clay microfabrics through this window using scanning electron microscope (SEM) and transmission electron microscope (TEM) techniques.

Acknowledgements

This research used samples and data provided by International Ocean Discovery Program (IODP). We thank the members of IODP expedition 351 Science Party and the captain and crew of the JOIDES Resolution. Shipboard bulk density and porosity measurements were performed by Mike Gurnis and Morihisa Hamada, and the anisotropy of magnetic susceptibility measurements on discrete samples by Matthew Meyer (Plymouth University).

Funding: This work was supported by the Natural Environment Research Council [grant number NE/M007367/1 awarded to AM]; and the European Research Council [grant number 306810, awarded to D.J.J. van Hinsbergen]. The paper benefitted from thoughtful reviews by Eric Ferré and an anonymous reviewer.

References

Acton, G. D., 2002. Paleomagnetic overprints in ocean sediment cores and their relationship to shear deformation caused by piston coring. J. Geophys. Res. 107, doi: 10.1029/2001JB000518.

Anson, G. L. and Kodama, K. P., 1987. Compaction-induced inclination shallowing of the post-depositional remanent magnetization in a synthetic sediment. Geophys. J. Int. 88, 673-692.

Arason, P. and Levi, S., 1990. Compaction and inclination shallowing in deep-sea sediments from the Pacific Ocean, J. Geophys. Res., 95(B4), 4501-4510, doi:10.1029/JB095iB04p04501.

Arculus, R. J., Ishizuka, O., Bogus, K. and the Expedition 351 Scientists, 2015a. Proceedings of the International Ocean Discovery Program Volume 351, doi:10.14379/iodp.proc.351.103.2015.

Arculus, R. J., Ishizuka, O., Bogus, K., Gurnis, M., Hickey-Vargas, R., Aljahdali, M. H., Bandini-Maeder, A. N., Barth, A. P., Brandl, P., Drab, L., do Monte Guerra, R., Hamada, M., Jiang, F., Kanayama, K., Kender, S., Kusano, Y., Li, H., Loudin, L. C., Maffione, M., Marsaglia, K. M., McCarthy, A., Meffre, S., Morris, A., Neuhaus, M., Savov, I. P., Sena, C., Tepley III, F. J., van der Land, C., Yogodzinski, G. M. and Zhang, Z., 2015b. A record of spontaneous subduction initiation in the Izu–Bonin–Mariana arc. Nat. Geosci. 8, 728–733, doi: 10.1038/ngeo2515.

Athy, L. F., 1930. Density, porosity and compaction of sedimentary rocks (abstract). American Association of Petroleum Geologists, Bulletin, 14, 24.

Bennett, R. H., Bryant, W. R. and Keller, G. H., 1981. Clay fabric of selected submarine sediments: fundamental properties and models. J. Sediment. Petrol. 51, 217-232.

Bennett, R. H., O'Brien, N. R. and Hulbert, M. H., 1991. Determinants of clay and shale microfabric signatures: processes and mechanisms. In: Bennett, R. H., Bryant, W. R. and Hulbert, M. H. (Eds.), Microstructures of Fine-grained Sediments from Mud to Shale. Springer-Verlag, New York, pp. 5 –32.

Bennett, R. H. and Hulbert, M. H., 1986. Clay Microstructure. Boston (International Human Resources Development Corp. Publ.).

Bjørlykke, K. and Høeg, K., 1997. Effects of burial diagenesis on stresses, compaction and fluid flow in sedimentary basins. Marine and Petroleum Geology, 14, 267-276.

Borradaile, G. J., 1988. Magnetic-susceptibility, petrofabrics and strain: Tectonophysics 156, 1–20, doi: 10.1016/0040-1951(88)90279-x.

Borradaile, G. J. and Jackson, M., 2004. Anisotropy of magnetic susceptibility (AMS): magnetic petrofabrics of deformed rocks. Geol. Soc. London Sp. Pub. 238, 299–360, doi: 10.1144/GSL.SP.2004.238.01.18.

Burmeister, K. C., Harrison, M. J., Marshak, S., Ferré, E. C., Bannister, R. A. and Kodama, K. P., 2009. Comparison of Fry strain ellipse and AMS ellipsoid trends to tectonic fabric trends in very low-strain sandstone of the Appalachian fold–thrust belt. J. Struct. Geol. 31, 1028-1038.

Curtis, C. D., Lipshie, S. R., Oertel, G. and Pearson, M. J., 1980. Clay orientation in some Upper Carboniferous mudrocks, its relationship to quartz content and some inferences about fissility, porosity and compactional history. Sedimentology 27, 333-339.

Deschamps, A. and Lallemand, S., 2003. Geodynamic setting of Izu-Bonin-Mariana boninites. Geol. Soc. London Sp. Publ. 219, 163–185, doi: 10.1144/GSL.SP.2003.219.01.08.

Dunlop, D. J. and Özdemir, Ö., 1997. Rock magnetism: fundamentals and frontiers. Cambridge University Press, Cambridge, 573 pp.

Hamilton, E. L., 1976. Variations of density and porosity with depth in deep sea sediments. Journal of Sedimentary Petrology, 46, 280-300.

Hirano, S., Ogawa, Y. and Kawamura, K., 2001. Deformation of unlithified sediments in an early stage of the compaction process deduced from microtextures and magnetic fabrics: ODP Leg 174B, Hole 1074A. In: Becker, K., Malone, M.J. (Eds.), Proc. ODPSci. Results, vol. 174B, 1 –13.

Hrouda, F., 1982. Magnetic anisotropy of rocks and its application in geology and geophysics. Geophys. Surveys 5, 37–82, doi: 10.1007/BF01450244.

Hrouda, F. and Jezek, J., 1999. Magnetic anisotropy indications of deformations associated with diagenesis. In: Tarling, D. H. and Turner, P. (eds), Palaeomagnetism and Diagenesis in Sediments, Geological Society, London, Special Publication, 151, 127-137.

Huang, W., Dupont-Nivet, G., Lippert, P. C., van Hinsbergen, D. J. J. and Hallot, E., 2013. Inclination shallowing in the Eocene Linzizong sediments from Tibet: correction, possible causes and implications for reconstructing the India-Asia collision. Geophys. J. Int. 194, 1390-1411.

Ishizuka, O., Taylor, R. N., Yuasa, M. and Ohara, Y., 2011a. Making and breaking an island arc: A new perspective from the Oligocene Kyushu-Palau arc, Philippine Sea. Geochem. Geophys. Geosys. 12, 1–40, doi: 10.1029/2010GC003440.

Ishizuka, O., Tani, K., Reagan, M. K., Kanayama, K., Umino, S., Harigane, Y., Sakamoto, I., Miyajima, Y., Yuasa, M. and Dunkley, D. J., 2011b. The timescales of subduction initiation and subsequent evolution of an oceanic island arc. Earth Planet. Sci. Lett. 306, 229–240, doi: 10.1016/j.epsl.2011.04.006

Ishizuka, O., Taylor, R. N., Ohara, Y. and Yuasa, M. , 2013. Upwelling, rifting, and age-progressive magmatism from the Oki-Daito mantle plume. Geology, 41, 1011–1014.

Jelínek, V., 1978. Statistical processing of anisotropy of magnetic susceptibility measured on groups of specimens. Studia Geophys. Geod. 22, 50–62, doi: 10.1007/BF01613632.

Jelínek, V., 1981. Characterization of the magnetic fabric of rocks. Tectonophysics 79, 63-67.

Johnson, C. L., Constable, C. G., Tauxe, L., Barendregt, R., Brown, L. L., Coe, R. S., Layer, P., Mejia, V., Opdyke, N. D., Singer, B. S., Staudigel, H. and Stone, D. B., 2008. Recent investigations of the 0-5 Ma geomagnetic field recorded by lava flows. Geochemistry, Geophys. Geosystems, *9*(4), doi:10.1029/2007GC001696.

Kawamura, K. and Ogawa, Y., 2002. Progressive microfabric changes in unconsolidated pelagic and hemipelagic sediments down to 180 mbsf, northwest Pacific, ODP Leg 185, Site 1149. In Ludden, J.N., Plank, T., and Escutia, C. (Eds.), Proc. ODP, Sci. Results, 185.

Kawamura, K. and Ogawa, Y., 2004. Progressive change of pelagic clay microstructure during burial process: examples from piston cores and ODP cores. Marine Geol. 207, 131-144. doi:10.1016/j.margeo.2004.03.016.

Kopf, A. and Behrmann, J. H., 1997. Fabric evolution and mechanisms of diagenesis in fine-grained sediments from the Kita-Yamato Trough, Japan Sea. J. Sedim. Res. 67, 590–600.

Larrasoaña, J. C., Pueyo, E. L. and Pares, J. M., 2004. An integrated AMS, structural, palaeo- and rock-magnetic study of Eocene marine marls from the Jaca-

Pamplona basin (Pyrenees, N Spain); new insights into the timing of magnetic fabric acquisition in weakly deformed mudrocks. Geol. Soc. London Sp. Publ. 238, 127–143, doi: 10.1144/GSL.SP.2004.238.01.10.

Locat, J. and Lee, H., 2002. Submarine landslides: Advances and challenges. Canadian Geotech. J. 39, 193–212.

Maffione, M., Pucci, S., Sagnotti, L. and Speranza, F., 2012. Magnetic fabric of Pleistocene continental clays from the hanging-wall of an active low-angle normal fault (Altotiberina Fault, Italy). Int. J. Earth Sci. 101, 849–861, doi: 10.1007/s00531-011-0704-9.

Maffione, M., Hernandez-Moreno, C., Ghiglione, M. C., Speranza, F., van Hinsbergen, D. J. J. and Lodolo, E., 2015. Constraints on deformation of the Southern Andes since the Cretaceous from anisotropy of magnetic susceptibility. Tectonophysics 665, 236–250, doi: 10.1016/j.tecto.2015.10.008.

Mondol, N. H., Fawad, M., Jahren, J. and Bjørlykke, K.,, 2008. Synthetic mudstone compaction trends and their use in pore pressure prediction. First Break, 26, 43-51.

Okino, K. and Fujioka, K., 2003. Central basin spreading center, Philippine Sea: Structure of an extinct spreading center and implications for marginal basin information. J. Geophys. Res. 108, 2040, doi:10.1029/2001JB001095.

Okino, Y., Shimakawa, Y. and Nagaoka, S., 1994. Evolution of the Shikoku Basin. J. Geomag. Geoelect. 46, 463–479.

Parés, J. M., 2015. Sixty years of anisotropy of magnetic susceptibility in deformed sedimentary rocks. Frontiers Earth Sci. 3, 1–13, doi: 10.3389/feart.2015.00004.

Potter, D. K. and Stephenson, A., 1988. Single-domain particles in rocks and magnetic fabric analysis. Geophysical Research Letters, 15, 1097-1100, doi: 10.1029/GL015i010p01097.

Reagan, M. K., Ishizuka, O., Stern, R. J., Kelley, K. A., Ohara, Y., Blichert-Toft, J., Bloomer, S. H., Cash, J., Fryer, P., Hanan, B. B., Hickey-Vargas, R., Ishii, T., Kimura, J. I., Peate, D. W., Rowe, M. C. and Woods, M., 2010. Fore-arc basalts and subduction initiation in the Izu-Bonin-Mariana system. Geochem. Geophys. Geosys., 11, 1–17, doi: 10.1029/2009GC002871.

Reynolds, S. and Gorsline, D.S., 1992. Clay microfabrics of deep sea mud(stones), California Continental Borderland. J. Sed. Petr. 62, 41-53.

Rochette, P., Jackson, M. and Aubourg, C., 1992. Rock Magnetism and the interpretation of magnetic susceptibility. Reviews Geophys. 30, 209–226.

Sagnotti, L. and Speranza, F., 1993. Magnetic fabric analysis of the Plio-Pleistocene clayey units of the Sant'Arcangelo basin, southern Italy. Physics of the Earth and Planetary Interiors, 77, 165-176.

Sagnotti, L., Speranza, F., Winkler, A., Mattei, M. and Funiciello, R., 1998. Magnetic fabric of clay sediments from the external northern Apennines (Italy). Phys. Earth Planet. Int. 105, 73–93, doi: 10.1016/S0031-9201(97)00071-X.

Schwehr, K., Tauxe, L., Driscoll, N. and Lee, H., 2006. Detecting compaction disequilibrium with anisotropy of magnetic susceptibility. Geochem. Geophys. Geosys. 7, doi: 10.1029/2006GC001378.

Schlater, J. G. and Christie, P. A. F., 1980. Continental stretching: an explanation of the post-mid-Cretaceous subsidence of the Central North Sea basin. Journal of Geophysical Research, 85, 3711-3739.

Tarling, D. and Hrouda, F. (Eds.), 1993. Magnetic anisotropy of rocks. Springer Science & Business Media.
Tauxe, L. and Kent, D. V., 2004. A simplified statistical model for the geomagnetic field and the detection of shallow bias in paleomagnetic inclinations: was the ancient magnetic field dipolar? Timescales Paleomag. Field, 145, 101–115.
Terzaghi, K., 1925. Erdbaumechanik auf Bodenphysikalischer Grundlage. Franz Deuticke, Liepzig-Vienna, 274 p.

Figure captions

Figure 1. (a) Location map of the Philippine Sea Plate (PSP) showing the main geological structures and domains inferred from bathymetry, and the location of IODP Site U1438. (b) Lithostratigraphic log from Site U1438. The grain size is averaged over 5 m thick intervals. (cl) clay; (si) silt; (vfs-fs) very fine to fine sand; (ms-vcs) medium to very coarse sand; (gr), granules. Unit subdivision is indicated.

Figure 2. (a-c) Anisotropy of magnetic susceptibility results from 173 discrete cubic samples from Unit I, IODP Hole U1438B, showing the variation with depth of (a) the corrected anisotropy degree, P_J (b) the shape parameter, T, and (c) mean susceptibility. (d-g) Variation with depth of physical property and lithostratigraphic data from IODP Expedition 351 shipboard measurements (Arculus et al., 2015a). (d) Density and porosity data from discrete samples. (e) Age model based on magnetostratigraphy. Each point on the age-depth curve represents a reversal of the magnetic polarity in the core dated using the reference geomagnetic polarity time scale (GPTS). Sedimentation rates are calculated on the basis of the magnetostratigraphy. (f) Simplified lithostratigraphic log of Unit I. (g) Proxy for quartz content derived from peak intensities on X-Ray diffraction spectra (note arbitrary units). The two dotted gray lines bracket the interval in which anisotropy and physical parameters progressively change (here defined as the 'initial compaction window').

Figure 3. Stereographic equal area projections of the principal susceptibility axes from samples (a) above and (b) below 83 mbsf.

Figure 4. (a) High-temperature variation of low-field magnetic susceptibility during a complete heating-cooling cycle, showing a clear Curie temperature of ~580°C (heating curve). The cooling curve shows a slightly higher Curie temperature probably due to the oxidation of original magnetite to maghemite. (b) Isothermal remanent magnetization (IRM) acquisition curve from a representative sample showing presence of low coercivity magnetite. (c) Susceptibility vs. intensity of natural remanent magnetization (NRM) showing a linear relationship suggesting constancy of ferromagnetic mineralogy downhole.

Figure 5. Variation with depth of (a) inclination and (b) declination of the magnetic remanence in Unit I after alternating field (AF) demagnetization at 25

mT of archive half core sections (2 cm measurement interval; see Arculus et al. (2015b) for full description of methodology). Data are in geographic coordinates, after correction using FlexIT core orientation tool data. Declination and inclination vary downward due to the reversals of the geomagnetic field. (a) Inclination decreases significantly below core 9H (the effect is more visible in the normally magnetized intervals). (b) Declination varies within each core likely due to drilling-induced shear effects, particularly evident in cores 3H, 5H, 8H, and 13H. The shear effect is expected to be minimum at the bottom of each core. (c) Core distribution with depth from Hole U1438B.

Figure 6. Representative orthogonal vector plots of demagnetization data from intervals used for the calculation of the mean inclination. We select only those intervals in which 25 mT AF steps provide a reliable measure of the isolated characteristic remanent magnetization directions (i.e., declination and inclination of the 25 mT step is at an angle < 10° from the best fit line calculated using the 20-40 mT interval). Black (white) dots represent the declination (inclination) projection.

Figure 7. Variation of uniaxial vertical shortening derived from the density data of Figure 2d (open circles) compared to published theoretical compaction trends for clays and claystones. The two dotted gray lines bracket the interval in which anisotropy and physical parameters progressively change (here defined as the 'initial compaction window').

Table S1. Summary of anisotropy of magnetic susceptibility data from Unit I of IODP Hole U1438B.

Figure 1

Click here to download Figure: Figure_1_Map_Lithos.pdf

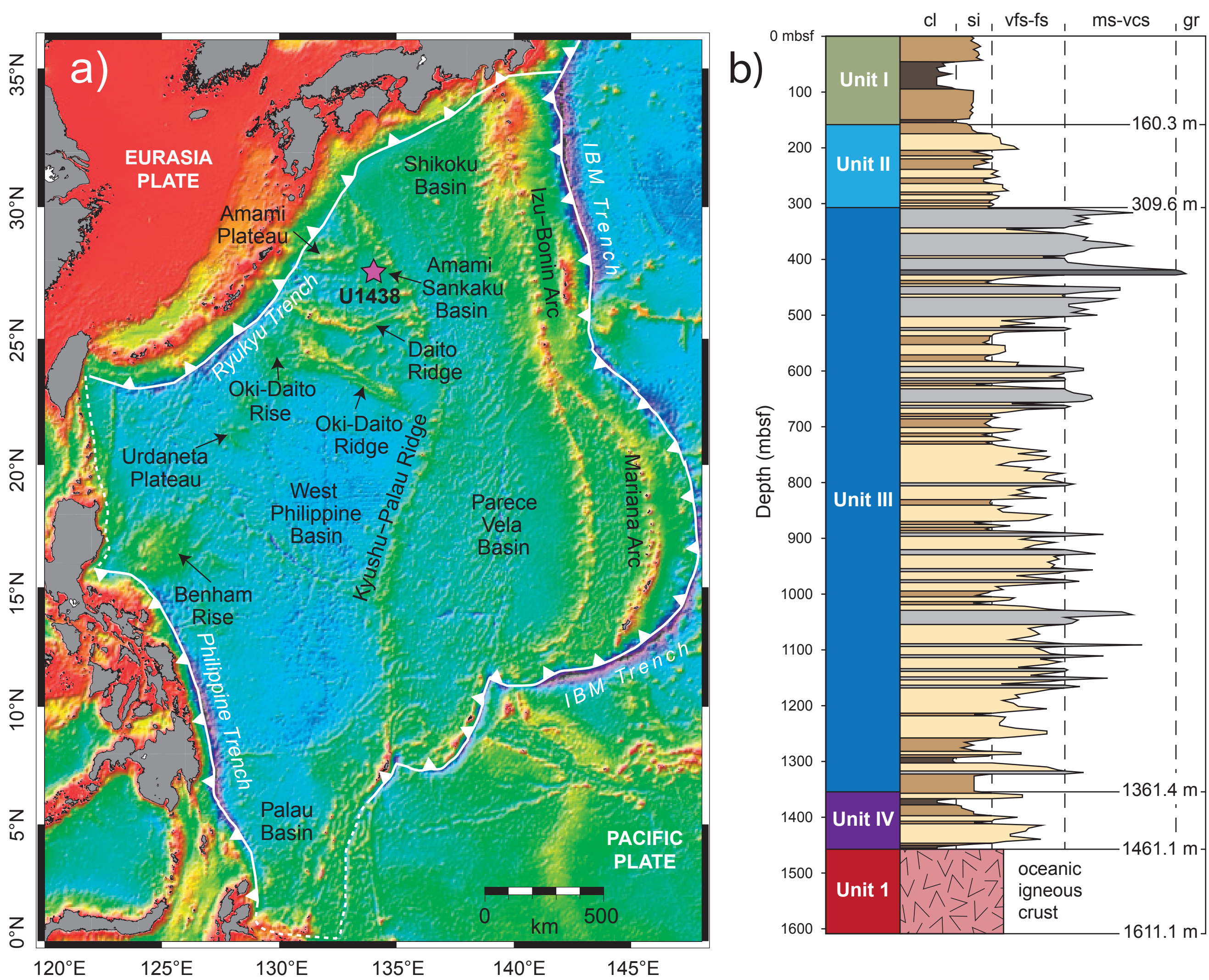

Figure 2

Click here to download Figure: Figure_2_Downhole_plots.pdf

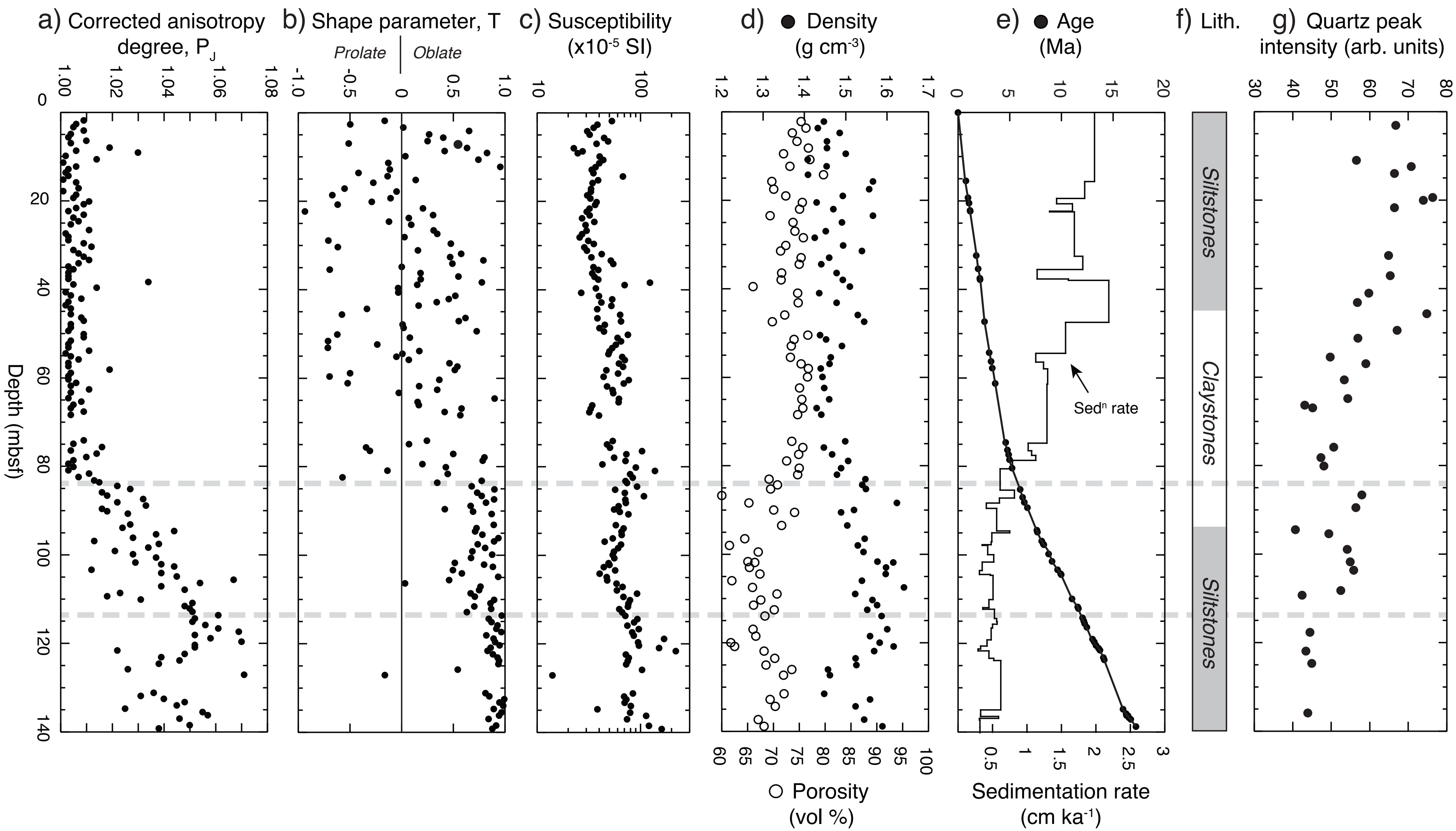

Figure 3

Click here to download Figure: Figure_3_AMS_stereonets.pdf

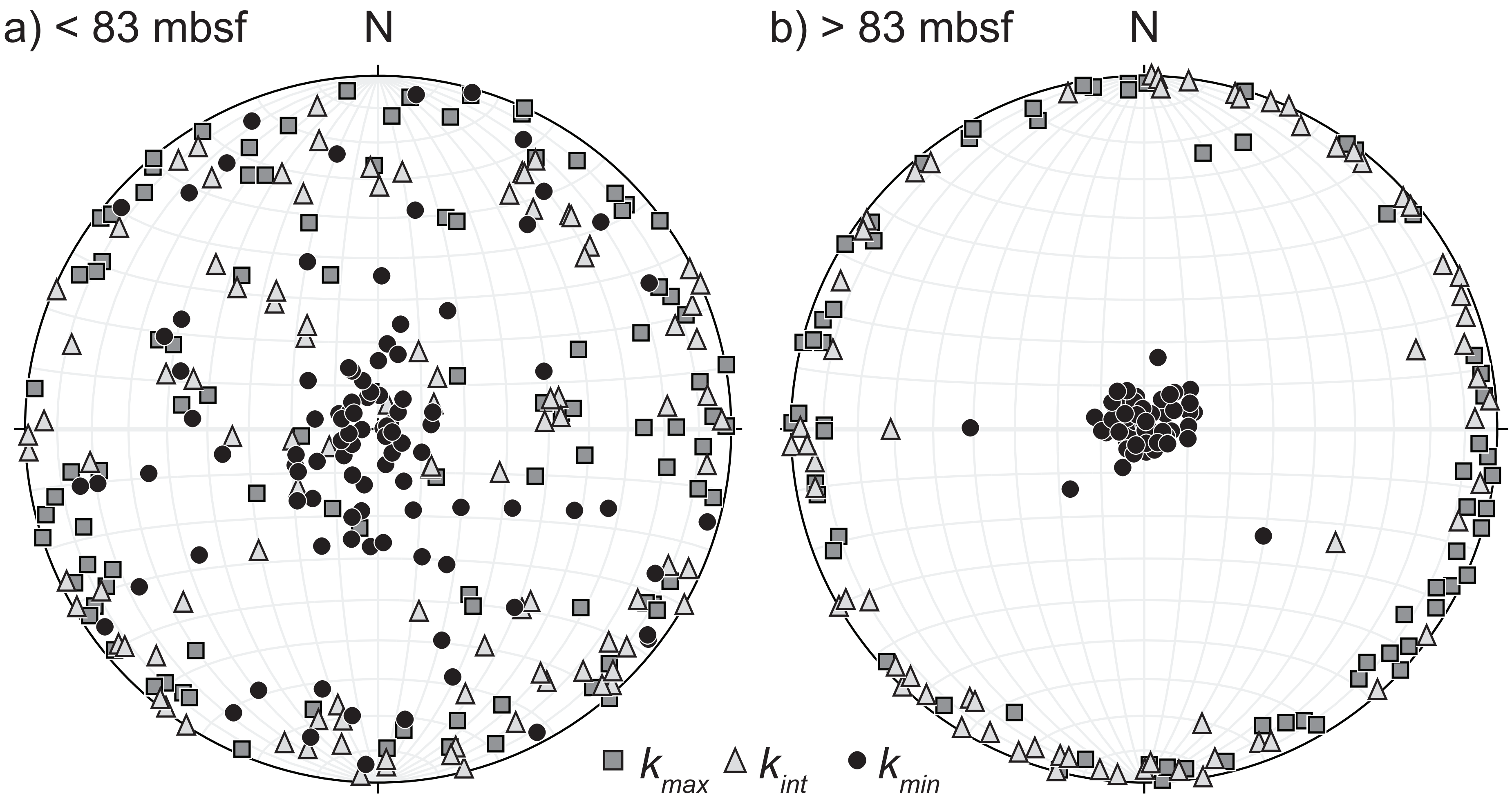

Figure 4

Click here to download Figure: Figure_4_Rock_magnetism.pdf

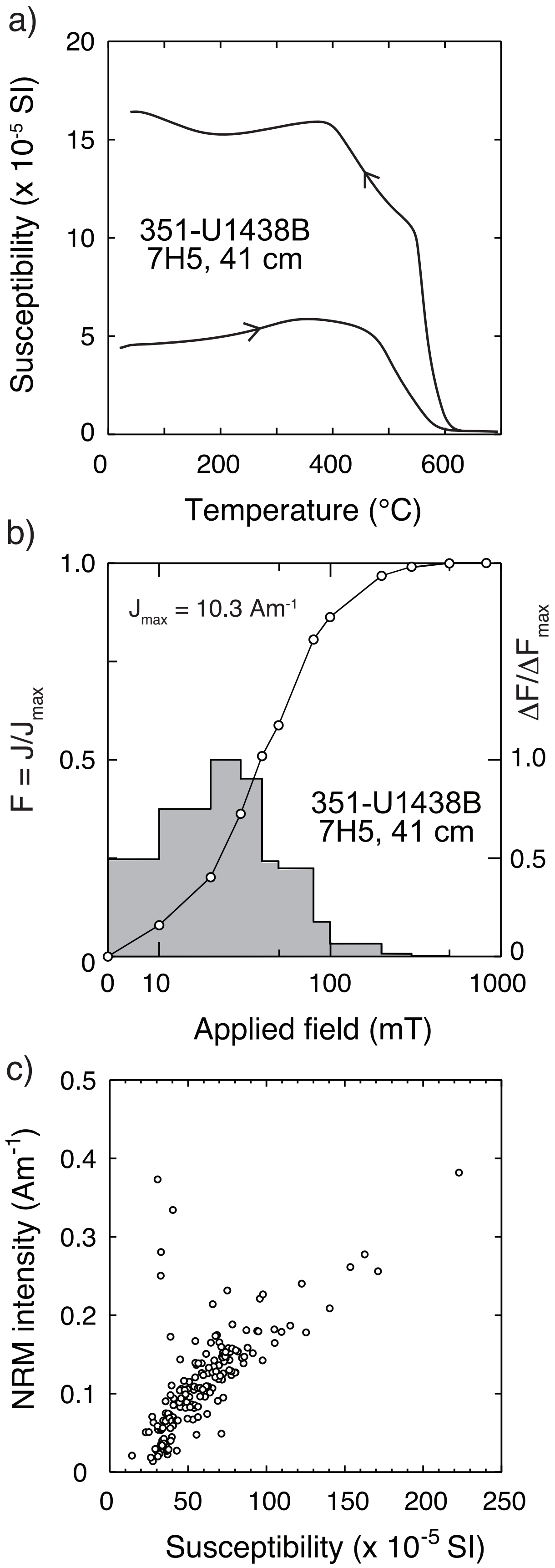

Figure 5

Click here to download Figure: Figure_5_Dec-Inc_plot.pdf

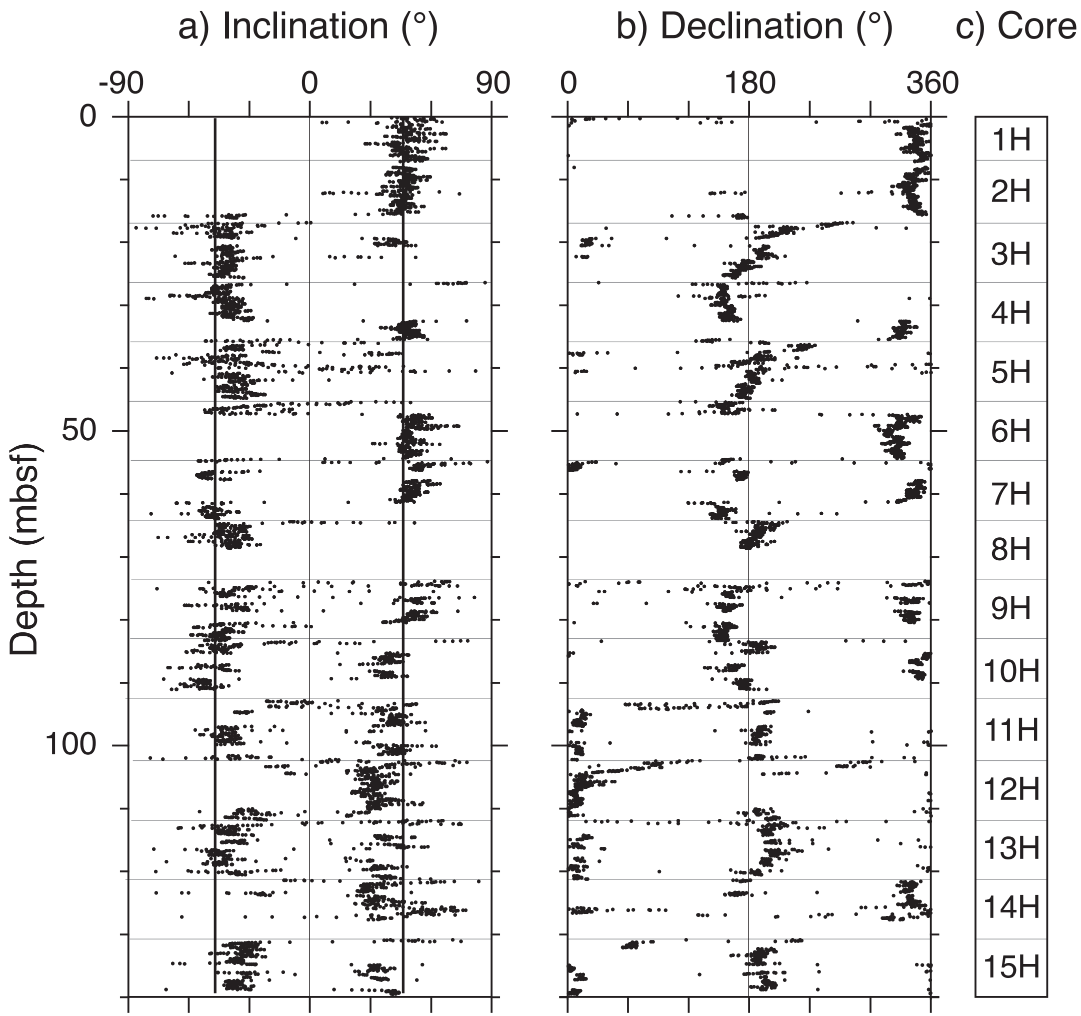

Figure 6

Click here to download Figure: Figure_6_Z-plots.pdf

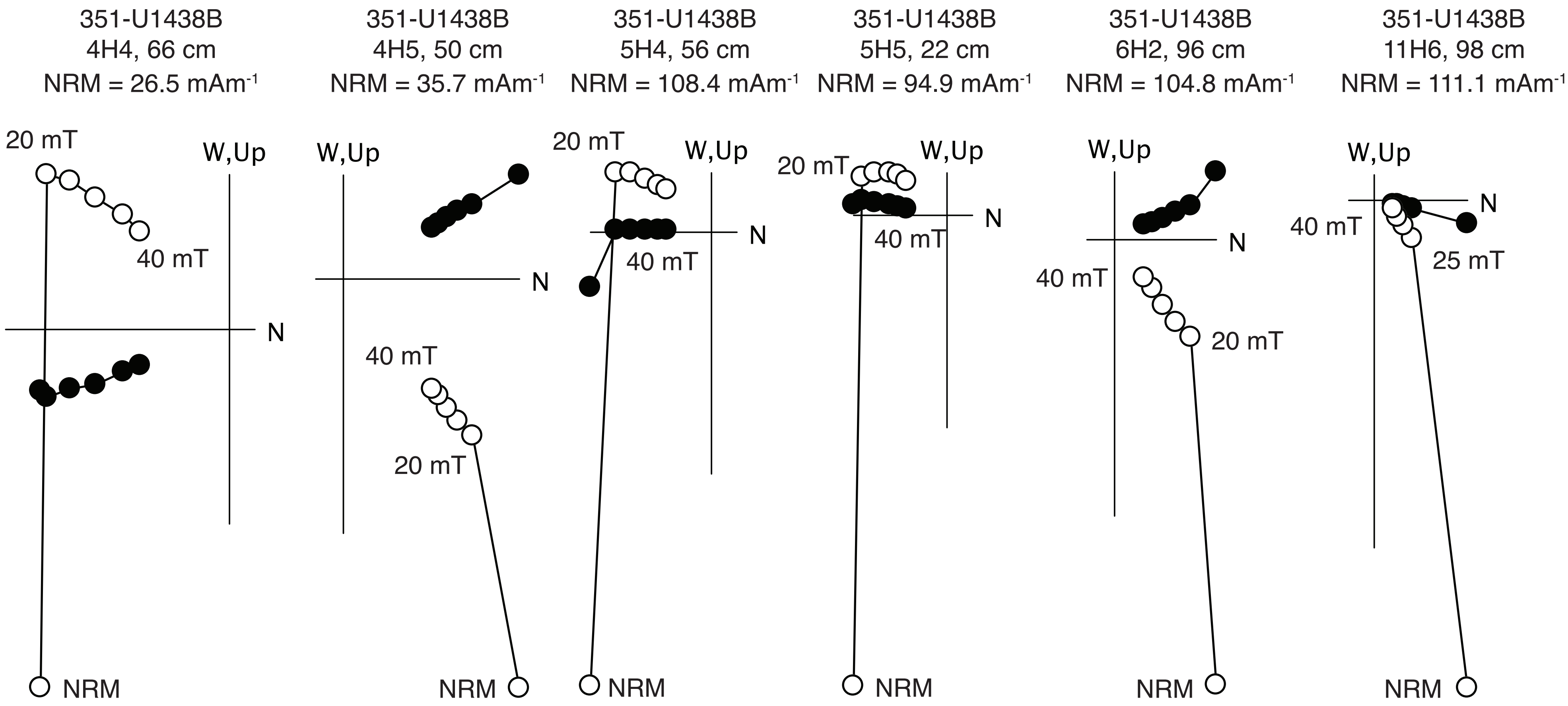

Figure 7
Click here to download Figure: Figure_7_Shortening_v_depth.pdf